HOKKAIDO UNIVERSITY

Title	Fixing Ni2+onto mesoporous SiO2-TiO2 through amino silane and application as a catalyst for Kumada cross coupling reaction for 1,1′ -biphenyl synthesis
Author(s)	Agustiningsih, Dewi; Otomo, Ryoichi; Kamiya, Yuichi et al.
Citation	Applied catalysis A : general, 672, 119606 https://doi.org/10.1016/j.apcata.2024.119606
Issue Date	2024-02-25
Doc URL	https://hdl.handle.net/2115/97185
Rights(URL)	https://creativecommons.org/licenses/by-nc-nd/4.0/
Type	journal article
File Information	Manuscript_Kamiya.pdf

Hokkaido University Collection of Scholarly and Academic Papers : HUSCAP

Submitted for publication in Applied Catalysis A: General

Fixing Ni^{2+} onto mesoporous SiO_2-TiO_2 through amino silane and application as a catalyst for Kumada cross coupling reaction for 1,1'-biphenyl synthesis

Dewi Agustiningsih[a,b], Ryoichi Otomo[c], Yuichi Kamiya[c,*], Nuryono Nuryono[a], Sri Juari Santosa[a], Eko Sri Kunarti[a,*]

[a]*Department of Chemistry, Faculty of Mathematics and Natural Sciences, Universitas Gadjah Mada, Sekip Utara, Yogyakarta 55281, Indonesia*

[b]*Graduate School of Environmental Science, Hokkaido University, Nishi 5, Kita 10, Kita-ku, Sapporo 060–0810, Japan*

[b]*Faculty of Environmental Earth Science, Hokkaido University, Nishi 5, Kita 10, Kita-ku, Sapporo 060–0810, Japan*

*Corresponding authors:

Yuichi Kamiya

Tel: +81 11-706 2217; E-mail: kamiya@ees.hokudai.ac.jp

Eko Sri Kunarti,

Tel: +62 815-7863-4638, E-mail: eko_kunarti@ugm.ac.id

Abstract

Biphenyl synthesis through cross coupling reaction holds significant importance in organic synthesis. In this research, development of heterogeneous Ni(II) catalyst for Kumada cross coupling reaction to produce 1,1'-biphenyl compounds was studied. We used mesoporous SiO_2-TiO_2 as support material and functionalized it with 3-aminopropyltriethoxylsilane (APTES) as a binding site, and then introduced Ni(II) as a catalytically active species. The synthesized catalysts were comprehensively characterized. Based on the results, it was concluded that the catalysts were successfully synthesized with Ni(II) being bound to amino group in APTES. The catalysts effectively promoted the reaction and the maximum yield of 92% with almost 100% selectivity was achieved at 50 °C and 6 h. The catalyst was reusable without severe deactivation in first reuse. Every components in the catalyst were indispensable for the catalyst to show high catalytic performance. The catalyst developed in this study exhibited the performance comparable to those of previously investigated catalysts.

Keywords: biphenyl, Kumada cross-coupling, nickel(II) catalyst, SiO_2-TiO_2, 3-aminopropyltriethoxysilane

1. Introduction

Many chemists and chemical engineers are currently interested in biphenyl production, because this chemical is served as a base compound to design high-affinity drugs such as antihypertensive and anticancer agents [1]. Additionally, biphenyl is commonly used as chemical intermediates in the production of agrochemicals, dielectric fluids in transformers and capacitors [2,3] as well as artificial flavours and fragrances [4]. In the synthesis of biphenyl, Kumada cross-coupling reaction is widely employed and homogeneous catalysts, specifically Ni(II)-phosphine complexes, are known to be excellent homogeneous catalysts to promote the reaction [5–9]. However, the use of homogeneous catalysts has several shortcomings, including difficulty in catalyst separation and low reusability. Furthermore, potential contamination of the final product with the catalyst must be avoided because it renders the homogeneous catalysts inadvisable for pharmacological synthesis [6,10–12]. Those inevitable problems with homogeneous catalysts can be overcome by replacing them with heterogeneous one, in which active species disperses on the surface of support materials.

In recent studies, heterogeneous catalysts were applied for the synthesis of biphenyl and its derivatives. Pd is one of the transition metals often employed as a catalyst in biphenyl synthesis. This metal has been used dispersing on diverse support materials, which include carboxymethyl cellulose/agar polysaccharides [13], Fe_3O_4 [14], SBA-15@adenin purine nucleobase [15], volcanic pumice magnetic particles@cellulose [16], cellulose@GO/Fe_3O_4 [17], and rGO@Fe_3O_4 [18], and all the catalysts gave biphenyl with extremely high yield. It should be mentioned, however, that the use of Pd catalysts is less economical because Pd is the metal with limited resources and thus is expensive. Consequently, if economically viable alternatives with similar catalytic activity exist, Pd is not the best choice. One of the low-cost transition metals applicable for biphenyl synthesis is Ni. Kiss et al. [6] explored the effectiveness of various transition metals supported on MgLaO as a catalyst and found that Ni

was the most efficient metal promoting this reaction and the maximum yield reached 86%. Similarly, Kiani and Naeimi [7] also investigated Ni as an active component, which was dispersed on $NiFe_2O_4$@SiO_2-BPMN, and the reaction over the catalyst produced a remarkable biphenyl yield of 97%.

In this study, we developed a novel heterogeneous Ni(II) catalyst and applied it for Kumada cross-coupling reaction to synthesize biphenyl. Ni(II) was used as a catalytically active metal ion, and was highly dispersed on mesoporous SiO_2-TiO_2 composite. Our motivation to choose silica as a base component of the support material was to expect many advantages on siliceous materials, including high surface area, large-size pores, high thermal stability, significant mechanical strength, abundant functional groups, and ease of availability [19]. In this study, rice husk ash extraction was used as an environmentally friendly and inexpensive silica source, and contained high purity silica, exceeding 90% [20–24]. Nonetheless, silica has a critical drawback as support material, which is insignificant affinity with transition metal ions that limit their fixation [19]. We thought that this problem could be addressed by combining silica with other metal oxides that have high affinity for metal ions, and one of them is titania. Because TiO_2 is known to be able to strongly interact with a wide variety of transition metal ions such as Au(III), Cu(II), Cu(I), Ni(II), Mn(II), Pd(II), Co(II), Co(III), and Ru(III) [25], and was observed to give significant role as support material in heterogeneous catalysts for coupling reactions [26–30]. However, TiO_2 also has some limitations such as low surface area, low thermal stability, and high agglomeration tendency [31,32]. Therefore, it was expected that the combining silica and titania would compensate for the shortcomings of each component, giving a support material with high thermal stability, high surface area, and high efficacy for catalytically active metal ions. In addition, we designed porosity in SiO_2-TiO_2 composite with pore size ranging from 2 to 50 nm, namely mesopores. This strategic design was conducted to exploit the benefits of meso-porosity in support

materials comprising their unique framework, high surface area, uniform pore size and shape, large pore volume, and ease of functionalization [33]. Furthermore, the mesoporous SiO_2-TiO_2 composite was modified with (3-aminopropyl)triethoxysilane (APTES) with aim to increase the amount of Ni(II) fixed on SiO_2-TiO_2 surface, hoping that amino group in APTES acted as a binding site for Ni(II) [34]. The use of APTES as linker agent in metals or metal ions-based catalysts had been investigated, usefulness of the compound for this purpose was demonstrated in some previous papers [35–38].

2. Experimental Section

2.1. Materials

All the chemicals used in this study were pro-analysis quality and were hydrochloric acid (37%, Sigma-Aldrich), NaOH (Sigma-Aldrich), 3-aminopropyltriethoxysilane (APTES, 99%, Sigma-Aldrich), $Ti[OCH(CH_3)_2]_4$ (97%, Sigma-Aldrich), PEG-40 (Merck), ethanol (99%, Merck and Wako), $NiCl_2 \cdot 6H_2O$ (99.9%, Merck), deoxygenated tetrahydrofuran (THF, 99.5%, Wako), C_6H_5MgBr in THF (16%, Wako), C_6H_5Br (98%, Wako), and tetradecane (99%, Wako). All water used in this study was Milli-Q water. The reagents and chemicals were used as received.

Rice husk ash was obtained from Yogyakarta, Indonesia.

2.2. Instrumentation

The materials characterization was performed using an attenuated total reflectance-infrared spectrometer (NICOLET iS10 PIKE GladiATR, Thermo Scientific), a powder X-ray diffractometer (D2 PHASER 2nd Generation, Bruker), a field emission-scanning electron microscope (S4800, HITACHI), a scanning transmission electron microscope-energy dispersive X-ray spectroscopy (HD-2000, HITACHI), a thermogravimetric analyser (Thermo

plus EVO2 TG-DTA8122, Rigaku), a surface area analyser (BELSORP-mini II, Microtrac), a transmission electron microscope (JEM-1400Plus, JEOL), an inductively coupled plasma-atomic emission spectrometer (ICPE-9000, Shimadzu), a X-ray photoelectron spectrometer (AXIS Supra^{+}, Shimadzu), and a gas chromatograph equipped with a flame ionization detector and an auto sampler (GC-2025 and AOC-20i, Shimadzu).

2.3. Synthesis of mesoporous SiO_2-TiO_2 composite

First, rice husk ash was treated in hydrochloric acid to remove impurities as follows. Rice husk ash was added to 1 mol L^{-1} hydrochloric acid and the resulting suspension was stirred at room temperature for 2 h. The solid was collected by filtration and washed with Milli-Q water until the pH of the filtrate was around 7. Then, it was dried at 80 °C for 8 h and calcined in air at 550 °C for 5 h. The obtained solid is called purified rice husk ash.

Next, silica component was extracted as sodium silicate from the purified rice husk ash. The purified rice husk ash was added to 1 mol L^{-1} NaOH solution, and the mixture was stirred at 90 °C for 2 h. After that, the resulting gel was collected by centrifugation. The obtained solid, which was mainly sodium silicate, was used as silica source for SiO_2-TiO_2 composite in the next step.

The synthesis of mesoporous SiO_2-TiO_2 composite was performed as follows. To the obtained sodium silicate, 1 mol L^{-1} hydrochloric acid was added until pH of the solution became neutral, and silica gel was formed. Next, 1.5 mL (0.005 mol) of $Ti[OCH(CH_3)_2]_4$ dispersed in 15 mL of ethanol was added to the silica gel, and the mixture was sonicated using a ultrasonication bath (Ney ULTRAsonik) at room temperature for 10 min. To keep the temperature at room temperature, the water medium in the sonication bath was changed every 15 min. Subsequently, an aqueous solution of PEG-40, which was prepared by adding it to hot water in advance, was added to the gel and the mixture was sonicated at room temperature for

1 h. Then, the solid was separated by filtration and dried at 80 °C for 24 h. The obtained solid was dispersed in ethanol and the resulting suspension was sonicated at room temperature for 1 h to remove the organic template. The obtained solid (mesoporous SiO_2-TiO_2 composite) was then collected by filtration, washed with cold ethanol three times, and dried at 60 °C for 8 h.

2.4. Modification of the SiO_2-TiO_2 composite with APTES [39]

The obtained SiO_2-TiO_2 composite was modified with APTES as follows. The SiO_2-TiO_2 composite was added to ethanol containing APTES with mass ratio of 1:1 (w/w) to SiO_2-TiO_2. The resulting suspension was sonicated at room temperature for 2 h and further stirred at room temperature for 6 h. Then, the solid was collected by centrifugation and filtration, and was washed with ethanol and Milli-Q water three times for each. The obtained solid was dried at 60 °C for 12 h. This solid is called SiO_2-TiO_2@APTES.

2.5. Introduction of Ni(II) to SiO_2-TiO_2@APTES

One gram of SiO_2-TiO_2@APTES was dispersed in 10 mL of Milli-Q water, and 3, 5, 7, or 10 mmol of $NiCl_2 \cdot 6H_2O$ was added to the suspension. Then, the mixture was sonicated at room temperature for 3 h and the solid was collected by filtration and washed with Milli-Q water three times. Finally, the obtained solid was dried at 80 °C for 4 h. The resulting solid is represented as "SiO_2-TiO_2@APTES-Ni(II)_*x* mmol", where *x* represents the amount of $NiCl_2 \cdot 6H_2O$ added.

2.6. Evaluation of catalytic performance

The catalytic performances of SiO_2-TiO_2@APTES-Ni(II)_*x* for Kumada cross-coupling reaction were evaluated as follows. To a test tube, 1 mmol of phenylmagnesium bromide, 1 mmol of bromobenzene, 2 mL of deoxygenated THF, and 0.1 g of catalyst were

added, and the mixture was stirred at 40, 50, 60, 70, or 80 °C. After pre-determined time (1, 3, 6, and 12 h), the reaction mixture was taken using a syringe with a filter. The collected reaction solution was analyzed using GC-FID equipped with DB-17 column (Agilent J&W). For the quantitative analysis, tetradecane was used as an internal standard. The conversion, and yield of and selectivity to biphenyl were calculated based on GC-FID results by following equations.

$$\text{Conversion}=\frac{\text{reacted amount of reactant}}{\text{initial amount of reactant}}\times 100\%$$

$$\text{Yield of biphenyl}=\frac{\text{produced amount of biphenyl}}{\text{initial amount of reactant}}\times 100\%$$

$$\text{Selectivity to biphenyl}=\frac{\text{produced amount of biphenyl}}{\text{reacted amount of reactant}}\times 100\%$$

3. Results and discussion

3.1. Materials characterization

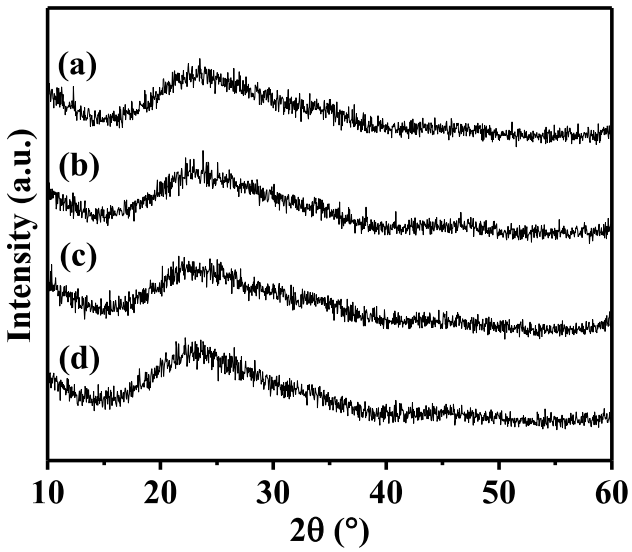

Fig. 1. XRD patterns of (a) SiO_2; (b) SiO_2-TiO_2; (c) SiO_2-TiO_2@APTES; (d) SiO_2-TiO_2@APTES-Ni(II)_10 mmol.

Fig. 1 shows XRD patterns of the synthesized materials including SiO_2, SiO_2-TiO_2, SiO_2-TiO_2@APTES, and SiO_2-TiO_2@APTES-Ni(II)_10 mmol. All the materials exhibited XRD patterns typical to amorphous with or without TiO_2, APTES, and Ni(II). Normally, titanium oxides tend to crystallize [40,41], but the synthesized SiO_2-TiO_2 was amorphous. This suggests that SiO_2 matrix inhibited crystallization of titanium oxides, in other words, TiO_x units were highly dispersed in SiO_2 matrix for the SiO_2-TiO_2. On the XRD pattern of SiO_2-TiO_2@APTES-Ni(II)_10 mmol, no diffraction line due to nickel oxides and nickel hydroxide was observed, suggesting that the added Ni(II) existed as isolated species likely attaching to amino group in APTES, forming coordination bond to the nitrogen atom. The immobilization of Ni(II) species on SiO_2-TiO_2@APTES-Ni(II)_10 mmol in a highly dispersed state was also confirmed by STEM-EDS measurement as shown in Figure S1.

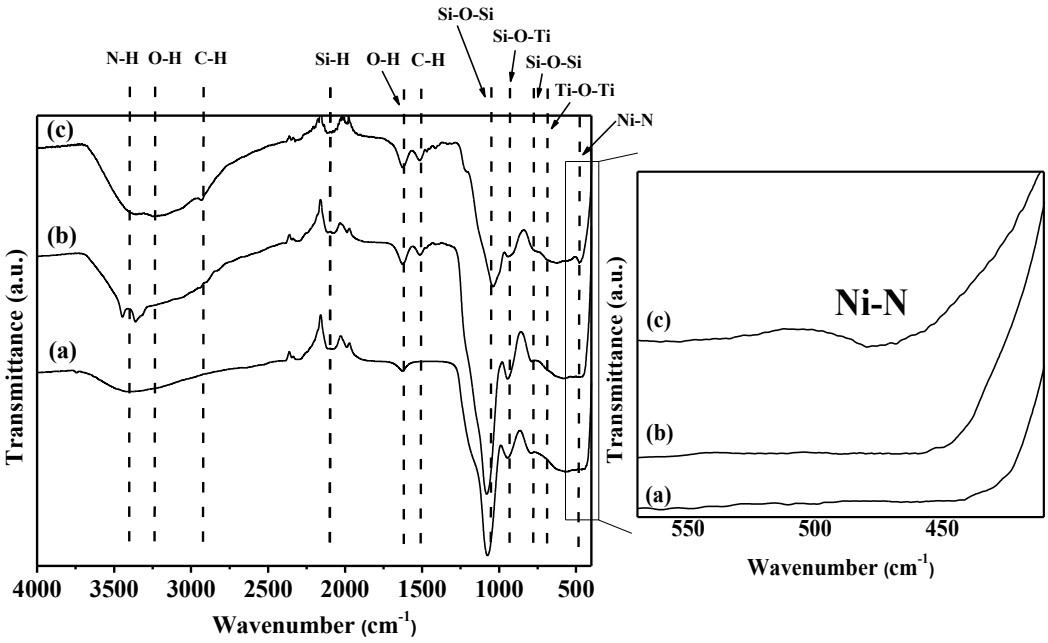

Fig. 2. IR spectra of (a) SiO_2-TiO_2; (b) SiO_2-TiO_2@APTES; (c) SiO_2-TiO_2@APTES-Ni(II)_10 mmol.

Fig. 2 shows IR spectra of SiO_2-TiO_2, SiO_2-TiO_2@APTES, and SiO_2-TiO_2@APTES_10 mmol. The SiO_2-TiO_2 gave a broad band due to surface OH group in the range of 3000-3400 cm^{-1}. In addition, strong absorption bands attributed to skeletal vibrations of SiO_2-TiO_2 [42,43] were observed in 700-1300 cm^{-1}. After the functionalization with APTES, new strong bands appeared at 3358 and 3443 cm^{-1} which were assigned to primary amino group. Besides, the presence of APTES was also affirmed by the bands at 2920 and 1495 cm^{-1}, which are stretching and bending vibrations of C-H bonds, respectively. The appearance of those bands demonstrated successful functionalization of SiO_2-TiO_2 with APTES. For the IR spectrum of SiO_2-TiO_2@APTES-Ni(II)_10 mmol, it should be noted that the bands due to primary amino group completely disappeared and instead a new band at 487 cm^{-1} appeared. According to the previous papers [44–48], this new band was attributable to Ni-N bond, suggesting that the nickel species was strongly attached on the surface through APTES. The disappearance of the two bands due to primary amino group by the introduction of Ni(II) was presumably caused by the strong perturbation to the amino group owing to the presence of Ni(II) attaching to the nitrogen atom. With the introduction of Ni(II), intensity of the absorption band at 2932 cm^{-1}, which was due to methylene group, was increased. This enhanced absorption was interpreted as follows; due to the formation of chemical bond between nitrogen atom in APTES and Ni(II), the electron density around nitrogen atom in APTES decreased, which was caused by the donation of an electron pair on nitrogen to Ni(II). This effect would give a perturbation to the C-H bond next to the nitrogen atom, resulting in strengthening the absorption due to methylene group.

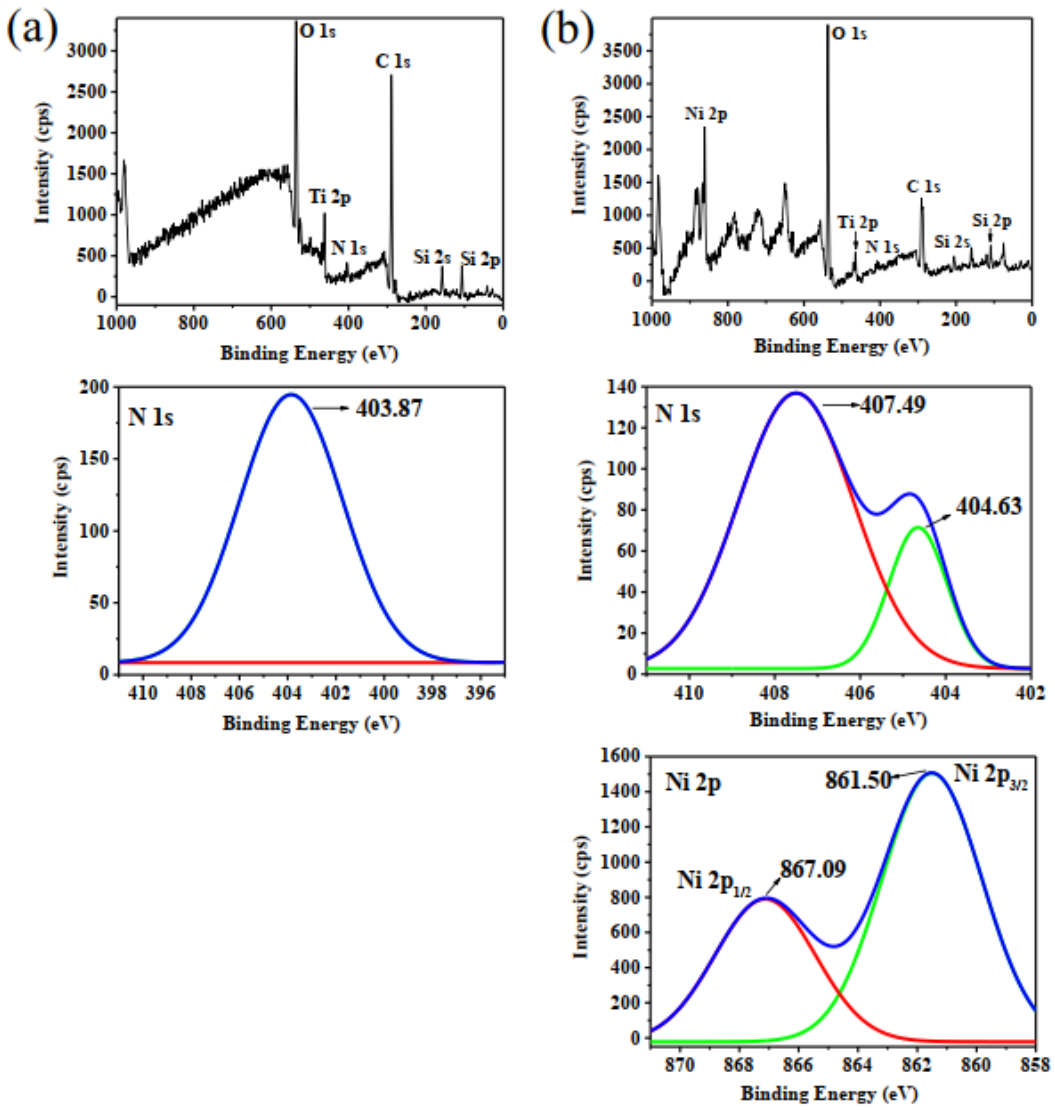

Fig. 3. Wide scan and narrow scan N1s XPS spectra of (a) SiO_2-TiO_2@APTES and (b) SiO_2-TiO_2@APTES-Ni(II)_10 mmol; narrow scan Ni2p spectrum of (b) SiO_2-TiO_2@APTES-Ni(II)_10 mmol.

Fig. 3 displays XPS spectra of SiO_2-TiO_2@APTES and SiO_2-TiO_2@APTES-Ni(II)_10 mmol, and deconvoluted curves. In the wide scan spectra of both samples, peaks of all elements that should exist were observed. Importantly, the peaks due to Ni existed only for SiO_2-TiO_2@APTES-Ni(II)_10 mmol, demonstrating that Ni(II) was successfully introduced onto the surface of SiO_2-TiO_2@APTES. Prior to Ni(II) introduction, namely SiO_2-TiO_2@APTES,

N1s peak displayed at 403.9 eV, which corresponded to neutral amino group. After the Ni(II) introduction, this peak split into two and the one was largely shifted to 407.5 eV, while binding energy (BE) of the other one remained almost the same as that before the Ni(II) introduction. The large shift in the direction of increasing BE means that nitrogen in the amino group was positively charged with the introduction of Ni(II) [39,49–51], which was a clear evidence for the presence of the strong interaction between Ni(II) and amino group. Additionally, Ni2p XPS spectrum of SiO_2-TiO_2@APTES-Ni(II)_10 mmol gave two peaks at 861.5 and 867. eV which were assigned to Ni(II) [52–55].

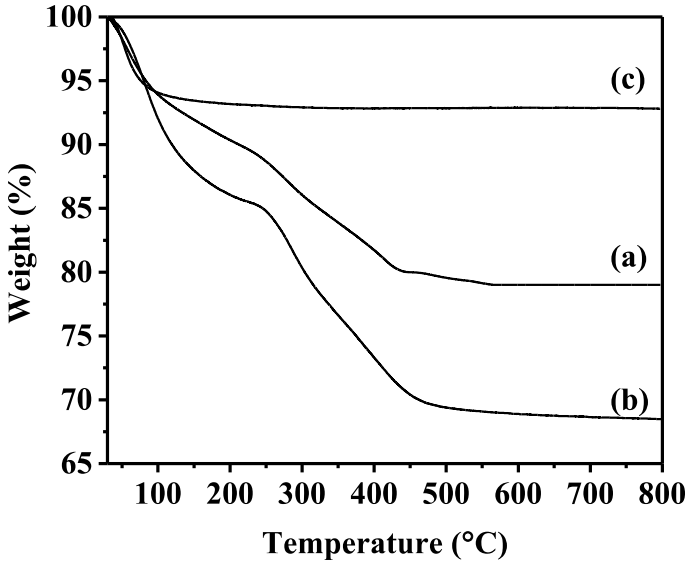

Fig. 4. TG curves taken in air up to 800 ºC for (a) SiO_2-TiO_2; (b) SiO_2-TiO_2@APTES; (c) SiO_2-TiO_2@APTES-Ni(II)_10 mmol.

Fig. 4 gives TG profiles taken in air for SiO_2-TiO_2, SiO_2-TiO_2@APTES and SiO_2-TiO_2@APTES_10 mmol. The SiO_2-TiO_2 lost the weight in three steps, being below 100 ºC, in 250-350 ºC, and over 400 ºC, though the temperature zones were not so clear. The first weight loss occurring below 100 ºC was due to desorption of physisorbed water and the next two were due to condensation of silanol and titanol groups. SiO_2-TiO_2@APTES lost about 30 wt%

weight at 800 ºC and such large weight loss was reasonably understood if excess APTES present in SiO_2-TiO_2@APTES was combusted by heating in air. For SiO_2-TiO_2@APTES_10 mmol, the weight loss at 800 ºC was only about 8%. Actually SiO_2-TiO_2@APTES_10 mmol had 6.5 mmol of Ni(II) (will be shown later), which corresponds to 0.49 g of NiO if it transforms to NiO. Since Ni(II) in SiO_2-TiO_2@APTES_10 mmol did not evaporate during TG measurement, but rather transformed into NiO, resulting in the only small weight loss of this material by heating. In other words, this small weight loss supported the successful introduction of Ni(II) to SiO_2-TiO_2@APTES.

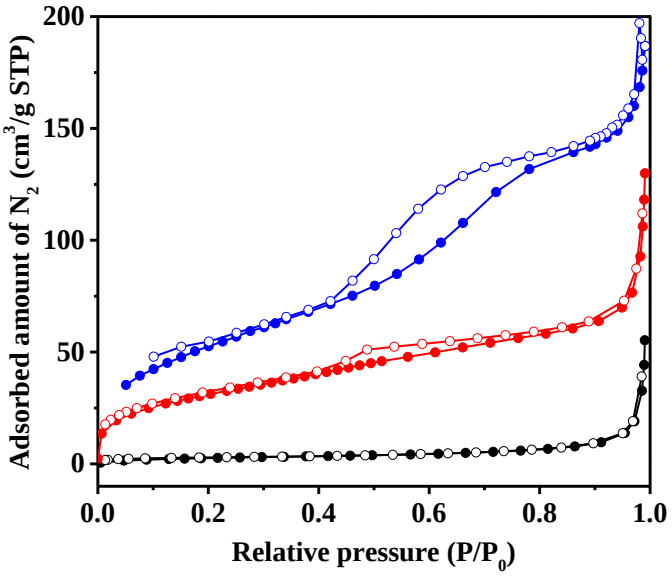

Fig. 5. N_2 adsorption-desorption isotherms of (●,○) SiO_2-TiO_2; (●,○) SiO_2-TiO_2@APTES; (●,○) SiO_2-TiO_2@APTES-Ni(II)_10 mmol.

Table 1. BET surface area and mesopore diameter of the samples estimated from N_2 adsorption-desorption isotherms.

Sample	BET surface area ($m^2\ g^{-1}$)	BJH pore diameter (nm)
SiO_2-TiO_2	228	22
SiO_2-TiO_2@APTES	10	---
SiO_2-TiO_2@APTES-Ni(II)_10 mmol	114	7

Fig. 5 displays N_2 adsorption-desorption isotherms of SiO_2-TiO_2, SiO_2-TiO_2@APTES, and SiO_2-TiO_2@APTES-Ni(II)_10 mmol. BET surface areas and pore diameters estimated from the isotherms are listed in Table 1. For SiO_2-TiO_2, large amount of N_2 was adsorbed at relatively low P/P_0 region and the isotherm showed type IV with a large hysteresis loop at P/P_0 > 0.4, indicating that the SiO_2-TiO_2 had high surface area and well-developed mesopores. In fact, BET surface area of the SiO_2-TiO_2 was large, being 228 m^2 g^{-1}. It is noted that the modification of SiO_2-TiO_2 with APTES caused significant decrease in the surface area and disappearance of the hysteresis loop on the N_2 adsorption-desorption isotherm of SiO_2-TiO_2@APTES. However, the introduction of Ni(II) to SiO_2-TiO_2@APTES giving SiO_2-TiO_2@APTES-Ni(II)_10 mmol led to recovery of the surface area, being 114 m^2 g^{-1}, and a hysteresis loop appeared again. Such recovery of the surface area with the introduction of Ni(II) implied that excess APTES present in the mesopores in SiO_2-TiO_2@APTES was removed in the process of the Ni(II) introduction.

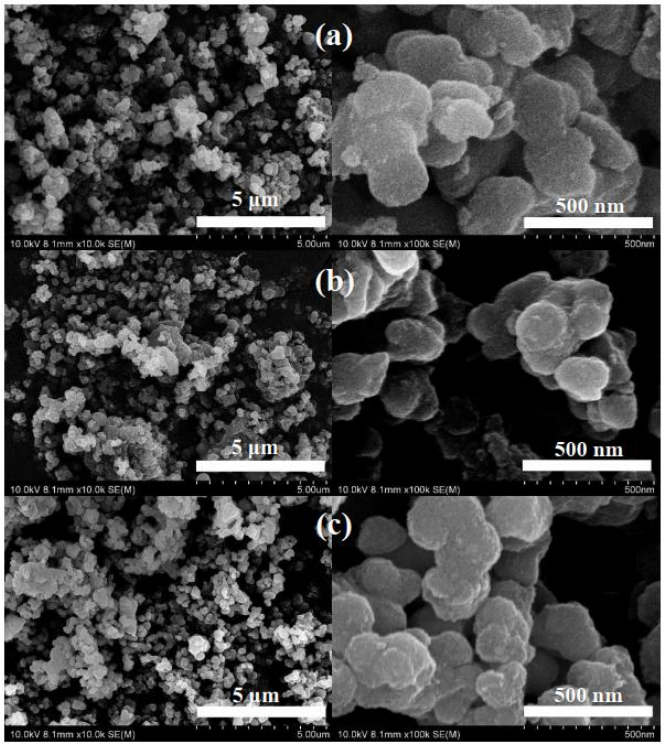

Fig. 6. SEM images of (a) SiO_2-TiO_2; (b) SiO_2-TiO_2@APTES; (c) SiO_2-TiO_2@APTES-Ni(II)_10 mmol. Magnification: left, ×10 k and right, ×100 k.

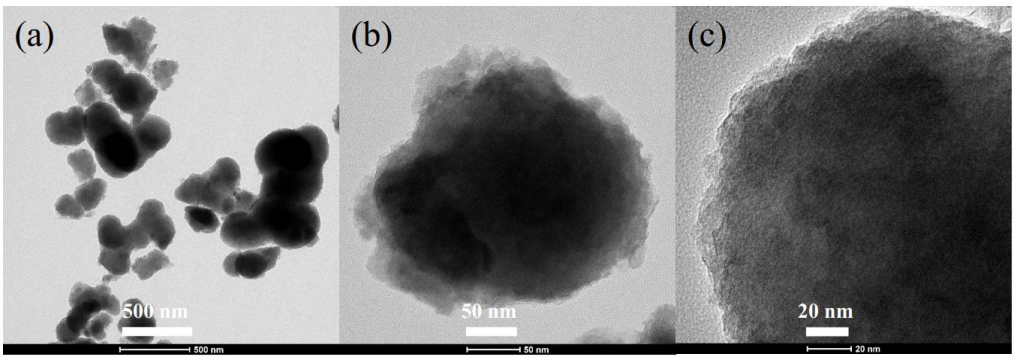

Fig. 7. TEM images of SiO_2-TiO_2@APTES-Ni(II)_10 mmol with different magnifications. Magnification: (a) ×100 k, (b) ×400 k, and (c) ×500 k.

The morphologies of SiO_2-TiO_2, SiO_2-TiO_2@APTES, and SiO_2-TiO_2@APTES-Ni(II)_10 mmol were observed by SEM. As Fig. 6a shows, SiO_2-TiO_2 had quasi-spherical shape with smooth surface. Such particle morphology was due to the effect of PEG-40 added as a template [56–58]. The particles were partly fused with the other ones, giving aggregates, due to high agglomeration tendency on amorphous phase like SiO_2 and TiO_2 [59]. The modification with APTES did not cause significant change in the particle morphology, while the surface became slightly textured (Fig. 6b). Even after the addition of Ni(II), no major change in particle morphology and size was observed (Fig. 6c). These results indicated that the modification of SiO_2-TiO_2 with APTES and subsequent introduction of Ni(II) occurred only on the surface, but did not change the bulk structure of SiO_2-TiO_2. Fig. 7 shows TEM images of SiO_2-TiO_2@APTES-Ni(II)_10 mmol with different magnifications. The TEM observations also showed that the particles of SiO_2-TiO_2@APTES-Ni(II)_10 mmol had quasi-spherical shape with quite high affinity of agglomeration between each other.

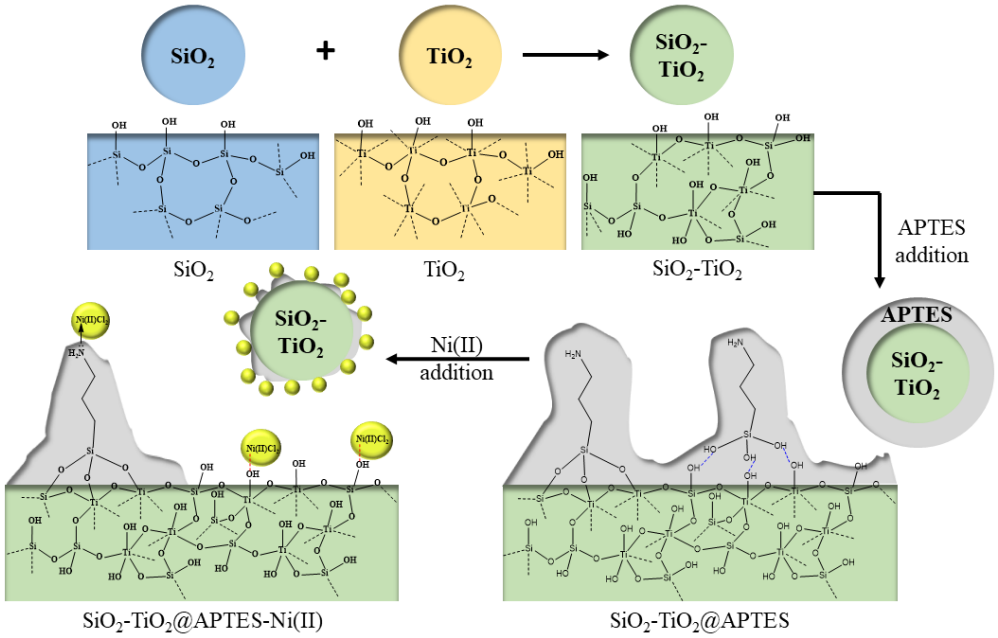

Fig. 8. Proposed structures of the synthesized materials at each step.

Based on those characterization data, the structures of the synthesized materials in each step are proposed as Fig. 8. The addition of titania to silica resulted in the formation of amorphous SiO_2-TiO_2 composite. This amorphous phase arose from the effective dispersion of titania within the silica matrix, thereby preventing crystallization of TiO_2. Subsequently, the surface of the amorphous SiO_2-TiO_2 composite was modified with APTES. In the process of the modification, ethoxide in APTES were condensed with silanol and titanol groups on the surface, and consequently APTES was strongly fixed on the surface through covalent bonds like Si-O-Si and Si-O-Ti. In addition to such strongly immobilized APTES, excess APTES was also present in SiO_2-TiO_2@APTES and those blocked the mesopores of SiO_2-TiO_2, significantly decreasing the surface area and mesopore volume. However, it is noted that during the Ni(II) introduction process, the excess APTES was removed. In SiO_2-TiO_2@APTES_Ni(II), Ni(II) species was fixed on the surface by the interaction with amino group on APTES. In addition to such Ni(II) species, some Ni(II) species might be present on the bare surface of SiO_2-TiO_2, while were minor one (will be discussed later).

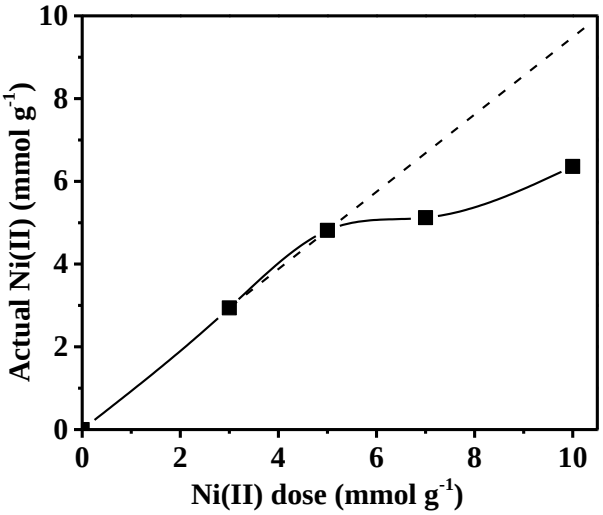

Fig. 9. Amount of actually introduced Ni(II) in SiO_2-TiO_2@APTES-Ni(II) prepared with different Ni(II) doses. Amount of actually introduced Ni(II) was determined by ICP-AES.

Fig. 9 shows the amount of actually introduced Ni(II) for SiO_2-TiO_2@APTES-Ni(II) prepared with different Ni(II) dose. The amount of actually introduced Ni(II) was increased with increase in the Ni(II) dose, but only a part of it was introduced when the Ni(II) dose exceeded 5 mmol g^{-1} and the amount seemed to approach the saturated value. In fact, SiO_2-TiO_2@APTES-Ni(II)_7 mmol and 10 mmol had only 5.1 and 6.4 mmol g^{-1} of Ni(II), respectively. Such trend is often observed for chemisorption, but not physisorption, and thus it can be said that Ni(II) species were strongly fixed on SiO_2-TiO_2@APTES-Ni(II) through chemical interaction.

3.2. Catalytic performances

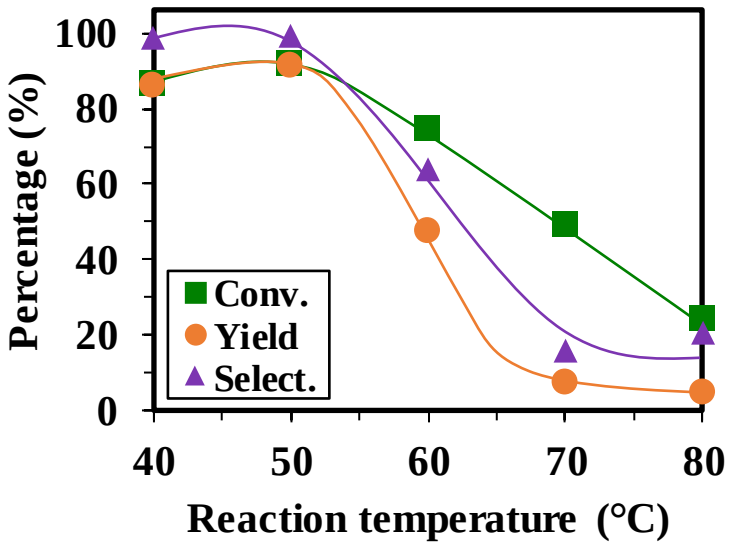

Fig. 10. Catalytic performance of SiO_2-TiO_2@APTES-Ni(II)_10 mmol for biphenyl synthesis at different reaction temperatures. Reaction conditions: catalyst, 0.1 g; reactants, PhMgBr and BrPh, 1 mmol each; solvent, deoxygenated THF, 2 mL; and time, 6 h.

Fig. 10 depicts the catalytic performance of SiO_2-TiO_2@APTES-Ni(II)_10 mmol at different reaction temperatures. At 40 °C, the catalyst showed 87.0% conversion and 86.5% yield of biphenyl with almost 100% selectivity. The conversion and yield were further increased at 50 °C while keeping the high selectivity. However, when the reaction temperature exceeded 60 °C or more, the catalytic performance deteriorated, that is to say, the catalyst was deactivated at the temperatures. In fact, the spent catalyst after the reaction at 80 °C showed only low catalytic performance when it was reused for the reaction at 50 °C, being 8.4% conversion and 4.9% yield. Therefore, we concluded that 50 °C was the optimal reaction temperature and subsequent reaction experiments were conducted at this temperature. A plausible reason for the catalyst deactivation occurring at high reaction temperature was

leaching of the active nickel species to reaction solution or forming the aggregate on the catalyst, though further investigations are still necessary.

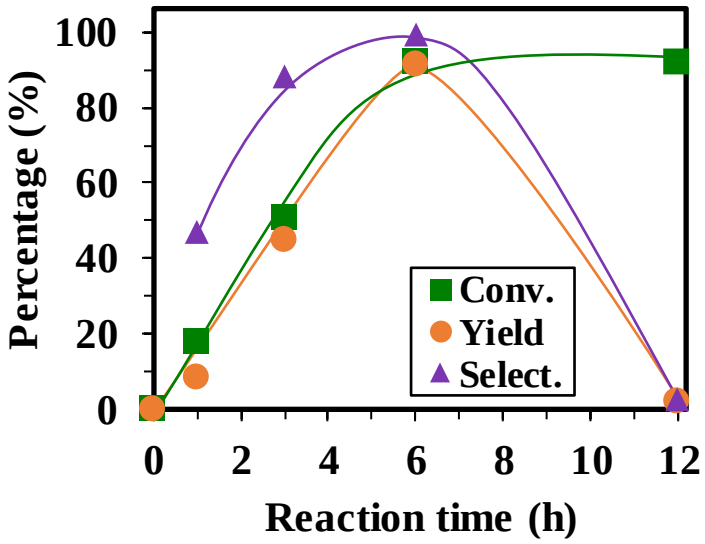

Fig. 11. Changes in conversion, yield, and selectivity over reaction time. Reaction conditions: catalyst, SiO_2-TiO_2@APTES-Ni(II)_10 mmol, 0.1 g; reactants, PhMgBr and BrPh, 1 mmol each; solvent, deoxygenated THF, 2 mL, and temperature, 50 °C.

Fig. 11 shows time-course changes in conversion, and yield of and selectivity to biphenyl in the reaction over TiO_2@APTES-Ni(II)_10 mmol. Conversion and yield were increased with increase in the reaction time up to 6 h. However, further prolongation of the reaction time rather decreased the yield. Since no product other than biphenyl was detected at 12 h by GC analysis, meaning significant decline in material balance. This phenomenon is explainable if nearly all products were strongly adsorbed on the catalyst surface in the prolonged reaction time. Therefore, we concluded that 6 h was the optimal reaction time. The reason for low selectivity observed in short reaction time especially at 1 h is still unclear, but reductive elimination of the reactive intermediates like diphenylnickel species to form the biphenyl was probably a rate-determining step since eventually the selectivity reached almost 100% at 6 h and no product other than biphenyl was detected whole the reaction time.

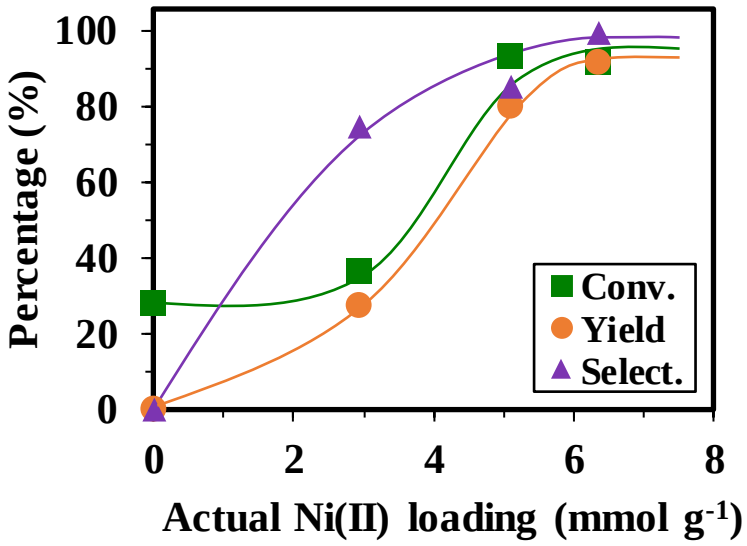

Fig. 12. Catalytic performances of SiO_2-TiO_2@APTES-Ni(II) with different Ni(II) loadings. Reaction conditions: catalyst, 0.1 g; reactants, PhMgBr and BrPh, 1 mmol each; solvent, deoxygenated THF, 2mL; temperature, 50 °C; and time, 6 h.

Next, we investigated influence of the Ni(II) loadings on the catalytic performances at optimal reaction temperature and time, which are 50 °C and 6 h, respectively. The results are provided in Fig. 12. The catalysts with Ni(II) gave biphenyl, while that without Ni(II), namely SiO_2-TiO_2@APTES, did not do at all, demonstrating that the Ni(II) species on SiO_2-TiO_2@APTES-Ni(II) formed active sites for the formation of biphenyl. The conversion and yield of biphenyl were increased with increase in the Ni(II) loadings and SiO_2-TiO_2@APTES-Ni(II)_10 mmol showed the best catalytic performance in terms of both activity and selectivity. In case of SiO_2-TiO_2@APTES-Ni(II)_10 mmol, while the turnover number with 0.1 g of the catalyst was 1.5 at 50 °C and 6 h, it increased to 6.9 with 0.01 g of the catalyst mass, which was calculated from 44% yield under the reaction conditions. Relatively low selectivity to biphenyl in the reaction over SiO_2-TiO_2@APTES-Ni(II)_3 mmol was probably because of the existence of the intermediates on the catalyst due to low conversion as mentioned before.

Table 2. Catalytic performances of all materials.

Catalyst	Conversion (%)	Yield (%)	Selectivity (%)
SiO_2-TiO_2@APTES-Ni(II)_10 mmol	92	92	100
SiO_2@APTES-Ni(II)_10 mmol	74	65	88
SiO_2-TiO_2-Ni(II)_10 mmol	24	9	37
SiO_2	41	0	0
TiO_2	22	0	0
SiO_2-TiO_2	31	0	0
SiO_2-TiO_2@APTES	28	0	0
Blank experiment (without catalyst)	4	0	0
Homogeneous $Ni(PPh_3)_2(NO_3)_2$ catalyst	89	7	8

Reaction conditions: catalyst, 0.1 g; reactants, PhMgBr and BrPh, 1 mmol each; solvent, deoxygenated THF, 2 mL; temperature, 50 °C; and time 6 h.

We further investigated how much important each component in SiO_2-TiO_2@APTES-Ni(II) to the reaction was. Table 2 summarizes catalytic reaction data with various materials (catalysts) containing or not containing each component. SiO_2@APTES-Ni(II)_10 mmol, which did not have TiO_2, showed moderate activity and selectivity, but the catalytic performance was lower than SiO_2-TiO_2@APTES-Ni(II)_10 mmol, demonstrating that TiO_2 in SiO_2-TiO_2 matrix was important component to immobilize the active nickel species. The reaction with SiO_2-TiO_2-Ni(II)_10 mmol produced biphenyl, but both activity and selectivity were very low comparing with those for SiO_2-TiO_2@APTES-Ni(II)_10 mmol. The materials without Ni(II) did not show any activity for the formation of biphenyl. It should be noted that SiO_2-TiO_2@APTES-Ni(II)_10 mmol was much more active and selective than a homogenous $Ni(PPh_3)_2(NO_3)_2$ catalyst, while the conversion was comparable each other.

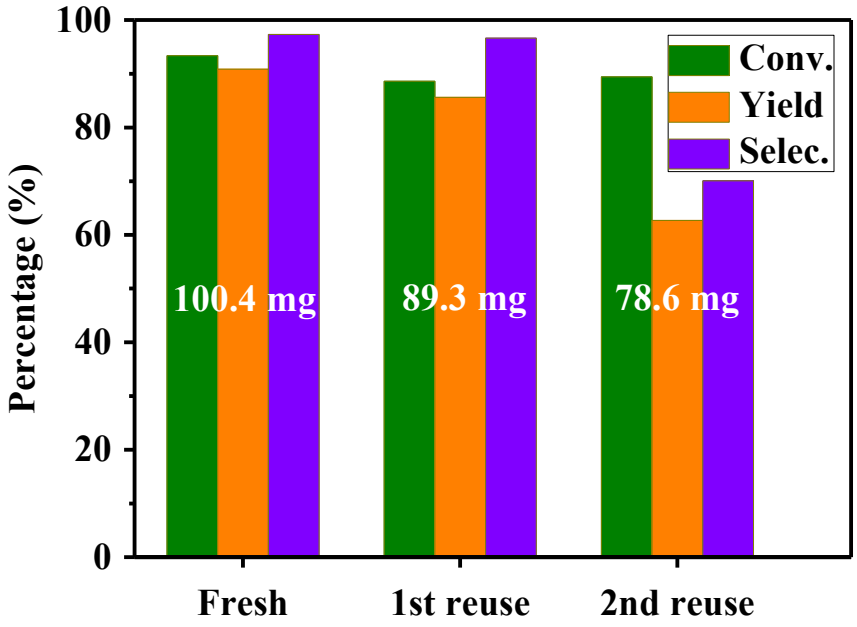

Fig. 13. Reusability test for SiO_2-TiO_2@APTES-Ni(II)_10 mmol. Reaction conditions: catalyst, 0.1 g; reactants, PhMgBr and BrPh, 1 mmol each; solvent, deoxygenated THF, 2 mL; temperature, 50 °C; and time, 6 h. After a reaction, catalyst was collected by filtration, followed by washing with water and ethanol, and then dried at 60 °C for 24 h. The values including 100.4, 89.3 and 78.6 mg shown on the bars in the figure represent catalyst amount used in each reaction.

We performed reusability test for SiO_2-TiO_2@APTES-Ni(II)_10 mmol. After a reaction, the catalyst was collected by filtration, washed with water and ethanol, and dried at 60 °C for 24 h and then it was afforded to a second reaction, which is called first reuse here. The results are shown in Fig. 13. For the first reuse, no significant decrease of the catalytic performance was observed. However, for the second reuse to the reaction, the selectivity to biphenyl was decreased, resulting in deterioration of the yield, while the conversion was almost the same as that for the previous two reactions.

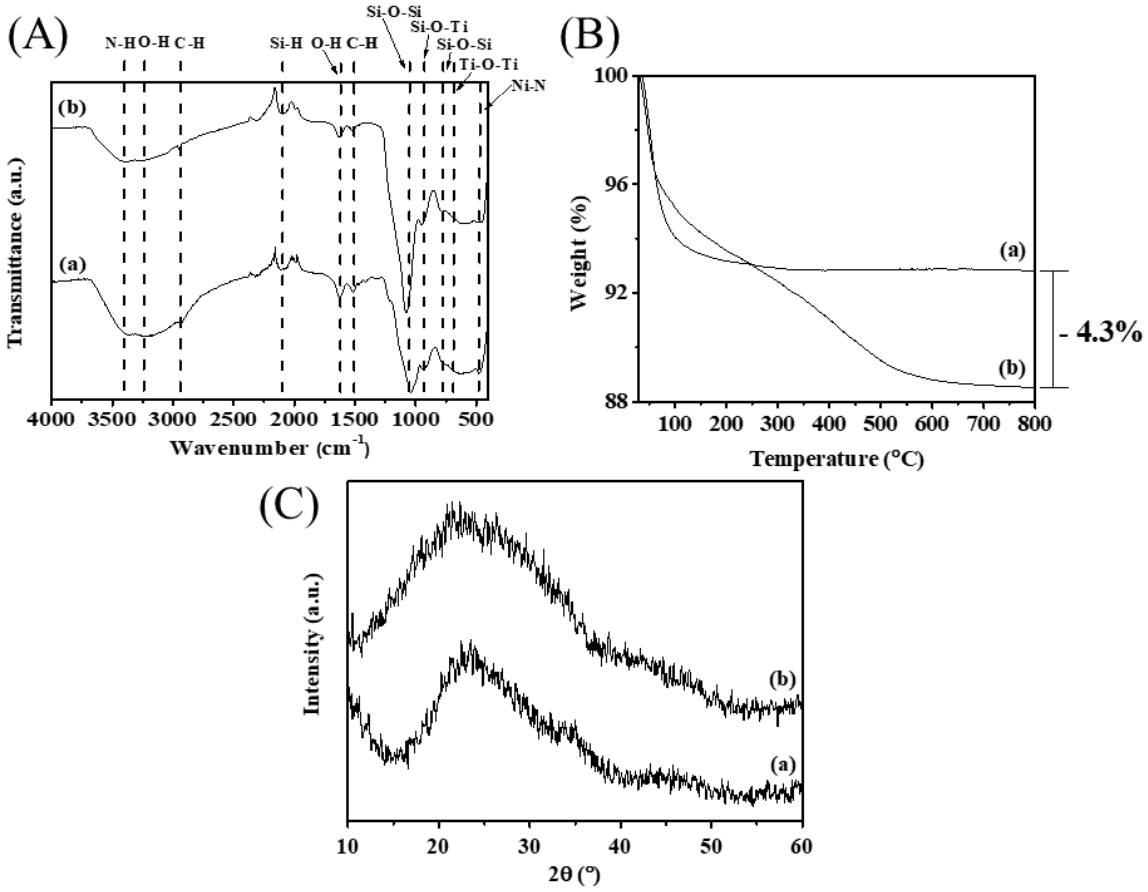

411
412 **Fig. 14.** Characterization results on (A) IR; (B) TGA; and (C) XRD for (a) fresh SiO_2-
413 TiO_2@APTES-Ni(II)_10 mmol; (b) the spent catalyst after the second reuse.

414

415 To know the reason for the catalyst deactivation, the spent catalyst after the second reuse were
416 characterized by IR, TGA, and XRD, and the resulting data were compared with those of the
417 fresh one. The results are shown in Fig. 14. On the IR spectrum of the spent catalyst, absorption
418 intensity of the band due to C-H stretching at 2932 cm^{-1} became stronger (Fig. 14A), suggesting
419 accumulation of organic compounds which was presumably the product. The accumulation of
420 the organic compounds was also confirmed from the TG profile of the spent catalyst (Fig. 14B).
421 The spent catalyst lost the weigh much more than the fresh one especially above 250 °C and
422 the difference in the weight losses between the fresh and spent catalysts at 800 °C was 4.4%.
423 In addition, slight agglomeration of Ni species was observed on the STEM-EDX mapping for
424 the spent catalyst (Figure S2). The bulk structure remained amorphous even for the spent

catalyst (Fig. 14c). Based on these results, it can be concluded that accumulation of the products on the catalyst, which was not removed by washing with water and ethanol, and agglomeration of Ni species caused the catalyst deactivation with repeated use.

Finally, we investigated substrate scope for Kumada cross coupling reaction over SiO_2-TiO_2@APTES-Ni(II)_10 mmol under the optimal reacion conditions. As Table S1 demonstrates, the catalyst showed moderate to high yields in the reactions of various substrates with electron-donating (methyl) and -withdrawing (nitro) substituents at *meta* and *para* positions. Especially, the catalyst was highly effective for the reaction of the substrates with electron-withdrawing substituent.

Table 3 summarizes previously reported catalytic performance data for Kumada cross-coupling reaction over supported Pd and Ni catalysts along with reaction conditions. Because the reaction conditions are different depending on the papers, we are not able to simply compare the catalytic performances, but we can conclude that our catalyst had the catalytic performance comparable to the previously reported catalysts. Thus, it is preferable to select Ni as an active component for the catalysts given that it is easier to obtain in nature and has less cost [8]. As consequence, though Ni is a bit lesser efficient than Pd, it is still more advantageous to be used as the active component for the synthesis of biphenyl by Kumada cross-coupling reaction.

Table 3. Comparison of the catalytic performance of SiO_2-TiO_2@APTES-Ni(II) with those of previously reported catalysts for synthesis of biphenyl by Kumada cross-coupling reaction.

Catalyst	Conditions	Yield	References
Fe_3O_4/o-PDA-Pd	r.t.; 10 min; 0.0064 mol% Pd catalyst; 1 mmol PhI; 1.2 mmol $PhB(OH)_2$; DCM*; sonication	98	[60]
Fe_3O_4@H_2L-Pd	100 °C; 10 min; 0.8 mol% Pd catalyst; 1 mmol PhI; 1 mmol $PhB(OH)_2$; water	99	[61]
Fe_2O_3@FLG@Pd	80 °C; 10 min; 4.8 10^{-6} mol% Pd catalyst; 1 mmol PhI; 1.2 mmol $PhB(OH)_2$; H_2O:EtOH (1:1); reflux	100	[62]
Fe_3O_4@GlcA@Ni-MOF	90 °C; 6 h; 0.18 mol% Ni catalyst; 1 mmol PhBr; 1 mmol $PhB(OH)_2$; water; reflux	88	[63]
LIS-Pd/TiO_2	60 °C; 10 min; 0.3 mol% Pd catalyst; 0.32 mmol PhBr; 0.38 mmol $PhB(OH)_2$; H_2O:EtOH (1:1); microwave irradiation	92	[29]
VPMP@CLS-Pd	r.t.; 10 min; 0.33 mol% Pd catalyst; 1 mmol PhI; 1.2 mmol $PhB(OH)_2$; DMSO*; reflux	98	[16]
Pd/Fe_3O_4	40 °C; 5 min; 0.1 mol% Pd catalyst; 1 mmol PhI; 1 mmol $PhB(OH)_2$; H_2O:EtOH (1:1); sonication	98	[14]
Ni^{2+}-MgLaO	r.t.; 3 h; 0.16 mol% Ni^{2+} catalyst; 10 mmol PhBr; 10 mmol PhMgBr; DE*; reflux	86	[6]
$NiFe_2O_4$@SiO_2–BPMN–Ni	r.t.; 40 min; 8 mol% Ni catalyst; 1 mmol PhI; 1.2 mmol $PhB(OH)_2$; H_2O:EtOH (1:1); sonication	97	[7]
SiO_2-TiO_2@APTES-Ni(II)	50 °C; 6 h; 0.064 mol% Ni^{2+} catalyst; 1 mmol PhBr; 1 mmol PhMgBr; THF*; stirring and heating	92	This work

*DCM, dichloromethane; DMSO, dimethyl sulfoxide; DE, diethyl ether; and THF, tetrahydrofuran.

Lastly, the reaction mechanism for Kumada cross-coupling reaction over SiO_2-TiO_2@APTES-Ni(II) is briefly explained based on previous reports [64,65] and shown in Fig.

15. In the first step, the reaction starts from transmetalation between two phenylmagnesium bromide with Ni(II) (Step 1). This step firstly leads to the release of biphenyl by reductive elimination of the attached two phenyl groups from Ni(II), and Ni(0) species is formed (Step 2). After that, Ni(0) undergoes oxidative addition with bromobenzene to form bromo(phenyl)nickel complex (Step 3). It is then continued with transmetalation between that complex and phenylmagnesium bromide giving diphenylnickel species (Step 4). Finally, reductive elimination to form biphenyl occurs and Ni(0) species is regenerated (Step 5).

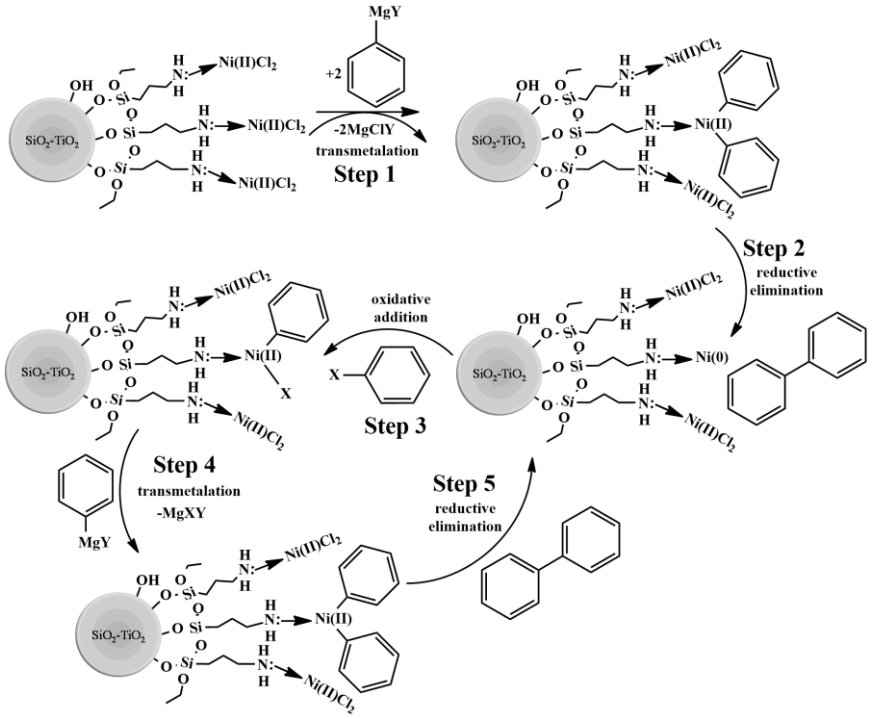

Fig. 15. Plausible reaction mechanism for Kumada cross-coupling reaction over SiO_2-TiO_2@APTES-Ni(II).

4. Conclusions

In this study, we successfully developed a novel heterogeneous Ni(II) catalyst that Ni(II) was introduced onto the mesoporous SiO_2-TiO_2 mainly through 3-aminopropyl triethoxysilane (APTES), in which Ni(II) was strongly immobilized on amino group in APTES.

The catalyst showed high activity and selectivity for Kumada cross coupling reaction to produce biphenyl and 92% yield with almost 100% selectivity was obtained under the optimum reaction conditions (50 °C and 6 h). All the components including SiO_2, TiO_2, APTES and Ni(II) were indispensable to give the catalyst high catalytic performance. The catalyst was able to be reused once, but the catalytic performance was decreased when reused for the second time probably because of the accumulation of the products. The catalyst that we developed showed the performance comparable to the previously reported heterogeneous Pd and Ni catalysts. Therefore, we concluded that our catalyst was one of the intriguing candidates practically applicable for the synthesis of biphenyl by Kumada cross-coupling reaction.

Acknowledgements

The work was supported by Ministry of Research, Technology, and Higher Education Indonesia (grant number 089/E5/PG.02.00/PT/2022; 1998/UN1/DITLIT/Dit-Lit/PT.01.03/2022; PMDSU scholarship) and Japan Student Services Organization (Student Exchange Support Program/Scholarship for Study in Japan under Agreement). We thank Prof. Noro in Hokkaido University for fruitful discussions and helpful comments.

We thank the Open Facility, Global Facility Center, Creative Research Institute, Hokkaido University for allowing us to conduct the analysis with ICP-AES and providing insight and expertise that greatly assisted the research. We also thank Ms. Nao Arai and Mr. Agora Chin in Hokkaido University for helping us to perform STEM-EDS analyses.

Conflict of interest

The authors disclose that they have no competing interests.

References

[1] L. Urquhart, Nat. Rev. Drug Discov. 17 (2018) 232. https://doi.org/10.1038/nrd.2018.42

[2] A. Buah-Kwofie, P.O. Yeboah, J. Pwamang, Chemosphere 82 (2011) 103–106. https://doi.org/10.1016/j.chemosphere.2010.09.063

[3] P. Thomas, J. CPRI 13 (2017) 621–628. Retrieved from https://cprijournal.in/index.php/pr/article/view/1028

[4] D.G. Brown, J. Boström, J. Med. Chem. 59 (2016) 4443–4458. https://doi.org/10.1021/acs.jmedchem.5b01409

[5] K. Bhowmik, D. Sengupta, B. Basu, G. De, RSC Adv. 4 (2014) 35442–35448. https://doi.org/10.1039/C4RA04834B

[6] Á. Kiss, Z. Hell, M. Bálint, Org. Biomol. Chem. 8 (2010) 331–335. https://doi.org/10.1039/B919246H

[7] F. Kiani, H. Naeimi, Ultrason. Sonochem. 48 (2018) 267–274. https://doi.org/10.1016/j.ultsonch.2018.06.001

[8] P.P. Nair, R.M. Philip, G. Anilkumar, Org. Biomol. Chem. 19 (2021) 4228–4242. https://doi.org/10.1039/D1OB00280E

[9] M.M. Heravi, V. Zadsirjan, P. Hajiabbasi, H. Hamidi, Monatsh. Chem. 19 (2019) 2236 https://doi.org/10.1002/tcr.201800190

[10] Á. Kiss, J. Németh, A. Fodor, Z. Hell, Period. Polytech. Chem. Eng. 59 (2015) 72–81. https://doi.org/10.3311/PPch.7343

[11] S. Vásquez-Céspedes, R.C. Betori, M.A. Cismesia, J.K. Kirsch, Q. Yang, Org. Process Res. Dev. 25 (2021) 740–753. https://doi.org/10.1021/acs.oprd.1c00041

[12] A. Ramesh, C.T. Da, R. Manigandan, P.B. Bhargav, M.T. Nguyen-Le, Colloids Interface Sci. Commun. 48 (2022) 100608. https://doi.org/10.1016/j.colcom.2022.100608

[13] T. Baran, Ultrason. Sonochem. 45 (2018) 231–237. https://doi.org/10.1016/j.ultsonch.2018.03.017

[14] H. Veisi, M. Ghorbani, S. Hemmati, Mater. Sci. Eng. C 98 (2019) 584–593. https://doi.org/10.1016/j.msec.2019.01.009

[15] T. Tamoradi, M. Ghadermazi, A. Ghorbani-Choghamarani, J. Porous Mater. 26 (2019) 121–131. https://doi.org/10.1007/s10934-018-0623-2

[16] S.S. Soltani, R. Taheri-Ledari, S.M.F. Farnia, A. Maleki, A. Foroumadi, RSC Adv. 10 (2020) 23359–23371. https://doi.org/10.1039/D0RA04521G

[17] M. Niakan, M. Masteri-Farahani, S. Karimi, H. Shekaari, J. Mol. Liq. 324 (2021) 115078. https://doi.org/10.1016/j.molliq.2020.115078

[18] V. Adimule, B.C. Yallur, M.M. Pai, S.R. Batakurki, S.S. Nandi, Top. Catal. (2022). https://doi.org/10.1007/s11244-022-01672-9

[19] M.E. Ali, M.M. Rahman, S.M. Sarkar, S.B.A. Hamid, J. Nanomater. (2014). https://doi.org/10.1155/2014/192038

[20] P. Deshmukh, J. Bhatt, D. Peshwe, S. Pathak, Trans. Indian Inst. Met. 65 (2012) 63–70. https://doi.org/10.1007/s12666-011-0071-z

[21] N. Setyawan, Hoerudin, S. Yuliani, IOP Conf. Ser. Earth Environ. Sci. 733 (2021). doi:10.1088/1755-1315/733/1/012149

[22] R. Yuvakkumar, V. Elango, V. Rajendran, N. Kannan, J. Exp. Nanosci. 9 (2014) 272–281. https://doi.org/10.1080/17458080.2012.656709

[23] P.P. Nayak, A.K. Datta, Silicon 13 (2021) 1209–1214. https://doi.org/10.1007/s12633-020-00509-y

[24] J.M. Mejía, R. Mejía De Gutiérrez, C. Montes, J. Clean. Prod. 118 (2016) 133–139. https://doi.org/10.1016/j.jclepro.2016.01.057

[25] S. Bagheri, N. Muhd Julkapli, S. Bee Abd Hamid, Sci. World J. (2014).

https://doi.org/10.1155/2014/727496

[26] J. De Tovar, F. Rataboul, L. Djakovitch, J. Catal. 398 (2021) 133–147. https://doi.org/10.1016/j.jcat.2021.04.016

[27] Y. Chen, K. Sun, T. Zhang, J. Zhou, Y. Liu, M. Zeng, X. Ren, R. Feng, Z. Yang, P. Zhang, B. Wang, X. Cao, Molecules 28 (2023). https://doi.org/10.3390/molecules28052399

[28] S. Pan, C. Gao, J. Gui, B. Hu, L. Gai, C. Qiao, C. Liu, Arab. J. Chem. 16 (2023) 104410. https://doi.org/10.1016/j.arabjc.2022.104410

[29] M.K. Das, J.A. Bobb, A.A. Ibrahim, A. Lin, K.M. Abouzeid, M.S. El-Shall, ACS Appl. Mater. Interfaces 12 (2020) 23844–23852. https://doi.org/10.1021/acsami.0c03331

[30] M.S.S. Adam, F. Ullah, M.M. Makhlouf, J. Am. Ceram. Soc. 103 (2020) 4632–4653. https://doi.org/10.1111/jace.17098

[31] R. Palcheva, L. Dimitrov, G. Tyuliev, A. Spojakina, K. Jiratova, Appl. Surf. Sci. 265 (2013) 309–316. https://doi.org/10.1016/j.apsusc.2012.11.001

[32] M. Ulfa, H. Al Afif, T.E. Saraswati, H. Bahruji, Materials 15 (2022) 1–13. https://doi.org/10.3390/ma15165471

[33] Y. Wu, Y. Zhang, J. Zhou, D. Gu, Emergent Mater. 3 (2020) 247–266. https://doi.org/10.1007/s42247-020-00086-1

[34] B. Jamwal, M. Kaur, H. Sharma, C. Khajuria, S. Paul, J.H. Clark, New J. Chem. 43 (2019) 4919–4928. 4919–4928. https://doi.org/10.1039/C8NJ05050C

[35] S. Rana, S. Maddila, K. Yalagala, S.B. Jonnalagadda, Appl. Catal. A Gen. 505 (2015) 539–547. http://dx.doi.org/10.1016/j.apcata.2015.07.018

[36] K.M. Parida, S. Mallick, P.C. Sahoo, S.K. Rana, Appl. Catal. A Gen. 381 (2010) 226–232. https://doi.org/10.1016/j.apcata.2010.04.008

[37] G.B.B. Varadwaj, S. Rana, K. Parida, J. Phys. Chem. C 118 (2014) 1640–1651.

https://doi.org/10.1021/jp410709n

[38] G.B.B. Varadwaj, S. Rana, K.M. Parida, Dalt. Trans. 42 (2013) 5122–5129. https://doi.org/10.1039/C3DT32495H

[39] Y. Bai, Z. Li, B. Cheng, M. Zhang, K. Su, RSC Adv. 7 (2017) 21758–21767. https://doi.org/10.1039/C6RA28098F

[40] T.D. Malevu, B.S. Mwankemwa, S. V. Motloung, K.G. Tshabalala, R.O. Ocaya, Phys. E Low-Dimensional Syst. Nanostructures 106 (2019) 127–132. https://doi.org/10.1016/j.physe.2018.10.028

[41] A.S. Bakri, M.Z. Sahdan, F. Adriyanto, N.A. Raship, N.D.M. Said, S.A. Abdullah, M.S. Rahim, AIP Conf. Proc. 1788 (2017). https://doi.org/10.1063/1.4968283

[42] D.C.L. Vasconcelos, V.C. Costa, E.H.M. Nunes, A.C.S. Sabioni, M. Gasparon, W.L. Vasconcelos, Mater. Sci. Appl. 02 (2011) 1375–1382. http://dx.doi.org/10.4236/msa.2011.210186

[43] J. Liu, Y. Zhang, Z. Wang, Y. Deng, P. Jian, L. Wang, R. Jian, J. Iran. Chem. Soc. 16 (2019) 1373–1381. http://dx.doi.org/10.1007/s13738-019-01611-8

[44] S.P. Roe, J.O. Hill, R.J. Magee, Monatshefte Für Chemie Chem. Mon. 122 (1991) 467–478. https://doi.org/10.1007/BF00809798

[45] J.M. Ramos, M.T. Mauŕicio, A.C. Costa, O. Versiane, C.A.T. Soto, ScienceAsia 37 (2011) 247–255. http://dx.doi.org/10.2306/scienceasia1513-1874.2011.37.247

[46] Waziri, Umaru, CSJ 11 (2020) 138–147. Retrieved from: https://www.ajol.info/index.php/csj/article/view/197396

[47] S.B. Ganjegaonkar, J.H. Deshmukh, P.A. Pawar, Orient. J. Chem. 38 (2022) 1018–1023. http://dx.doi.org/10.13005/ojc/380425

[48] G. Sanjay, Res. Rev. J. Chem. 2 (2013) 10–15. Retrieved from: https://www.rroij.com/open-access/nickel-complexes-of-thiosemicarbazone-

derivatives-of-lawsone-.php?aid=33868

[49] A. Calvo, L. Andrini, F.J. Williams, J.M. Ramallo-López, G.J.A.A. Soler-Illia, F.G. Requejo, J. Sol-Gel Sci. Technol. 102 (2022) 172–184. https://doi.org/10.1007/s10971-021-05579-x

[50] V.C. Karade, A. Sharma, R.P. Dhavale, R.P. Dhavale, S.R. Shingte, P.S. Patil, J.H. Kim, D.R.T. Zahn, A.D. Chougale, G. Salvan, P.B. Patil, Sci. Rep. 11 (2021) 1–12. https://doi.org/10.1038/s41598-021-84770-0

[51] A. Miranda, L. Martínez, P.A.A. De Beule, MethodsX 7 (2020). https://doi.org/10.1016/j.mex.2020.100931

[52] X. Hu, M. Zhang, A. Ren, Y. Huang, X. Yan, R. Feng, G. Zhao, Catal. Today 405–406 (2022) 75–81. https://doi.org/10.1016/j.cattod.2022.08.001

[53] X. Ning, Y. Lu, H. Fu, H. Wan, Z. Xu, S. Zheng, ACS Appl. Mater. Interfaces 9 (2017) 19335−19344. https://doi.org/10.1021/acsami.7b04100

[54] C. Cui, X. Zhao, X. Su, W. Gao, J. Zhan, X. Zhang, G. Li, X.L. Zhang, Y. Sang, H. Liu, J. Environ. Chem. Eng. 9 (2021). https://doi.org/10.1016/j.jece.2021.106416

[55] M.Z. Sarker, M.M. Rahman, H. Minami, T. Suzuki, H. Ahmad, Colloid Polym. Sci. 300 (2022) 279–296. 106416. https://doi.org/10.1007/s00396-021-04910-w

[56] P. Kumar, H. Khanduri, S. Pathak, A. Singh, G.A. Basheed, R.P. Pant, Dalt. Trans. 49 (2020) 8672–8683. https://doi.org/10.1039/D0DT01318H

[57] F. Branda, B. Silvestri, G. Luciani, A. Costantini, F. Tescione, Colloids Surfaces A Physicochem. Eng. Asp. 367 (2010) 12–16. https://doi.org/10.1016/j.colsurfa.2010.05.036

[58] R. Nandanwar, P. Ingh, F.F. Syed, F.Z. Haque, Orient. J. Chem. 30 (2014) 1577–1584. http://dx.doi.org/10.13005/ojc/300417

[59] Y. Tian, W. Jiao, P. Liu, S. Song, Z. Lu, A. Hirata, M. Chen, Nat. Commun. 10 (2019)

1–9. https://doi.org/10.1038/s41467-019-13054-z

[60] A. Maleki, R. Taheri-ledari, R. Ghalavand, R. Firouzi-haji, J. Phys. Chem. Solids 136 (2020) 109200. https://doi.org/10.1016/j.jpcs.2019.109200

[61] S.A. Jasim, M.J. Ansari, H.S. Majdi, M.J.C. Opulencia, K.F. Uktamov, J. Mol. Struct. 1261 (2022) 132930. 132930. https://doi.org/10.1016/j.molstruc.2022.132930

[62] F. Rafiee, P. Khavari, Z. Payami, N. Ansari, J. Organomet. Chem. 883 (2019) 78–85. https://doi.org/10.1016/j.jorganchem.2019.01.014

[63] A. Ghorbani-Choghamarani, Z. Taherinia, M. Mohammadi, Environ. Technol. Innov. 24 (2021) 102050. https://doi.org/10.1016/j.eti.2021.102050

[64] L. Iffland, A. Petuker, M. Van Gastel, U. Apfel, Inorganics 5 (2017) 78. https://doi.org/10.3390/inorganics5040078

[65] K. Tamao, K. Sumitani, M. Kumada, J. Am. Chem. Soc. 94 (1972) 4374–4376. https://doi.org/10.1021/ja00767a075

Supporting information

Fixing Ni^{2+} onto mesoporous SiO_2-TiO_2 through amino silane and application as a catalyst for Kumada cross coupling reaction for 1,1'-biphenyl synthesis

Dewi Agustiningsih[a,b], Ryoichi Otomo[c], Yuichi Kamiya[c,*], Nuryono Nuryono[a], Sri Juari Santosa[a], Eko Sri Kunarti[a,*]

[a]*Department of Chemistry, Faculty of Mathematics and Natural Sciences, Universitas Gadjah Mada, Sekip Utara, Yogyakarta 55281, Indonesia*

[b]*Graduate School of Environmental Science, Hokkaido University, Nishi 5, Kita 10, Kita-ku, Sapporo 060–0810, Japan*

[b]*Faculty of Environmental Earth Science, Hokkaido University, Nishi 5, Kita 10, Kita-ku, Sapporo 060–0810, Japan*

STEM-EDX mapping for fresh SiO_2-TiO_2@APTES-Ni(II)_10 mmol

To confirm the immobilization of Ni(II) species in a highly dispersed state, STEM-EDS measurement was performed. As shown in the EDS mapping of SiO_2-TiO_2@APTES-Ni(II)_10 mmol (Figure S1), the Ni species were homogeneously dispersed over the entire surface of the sample, and the distribution of the species was similar to that of carbon.

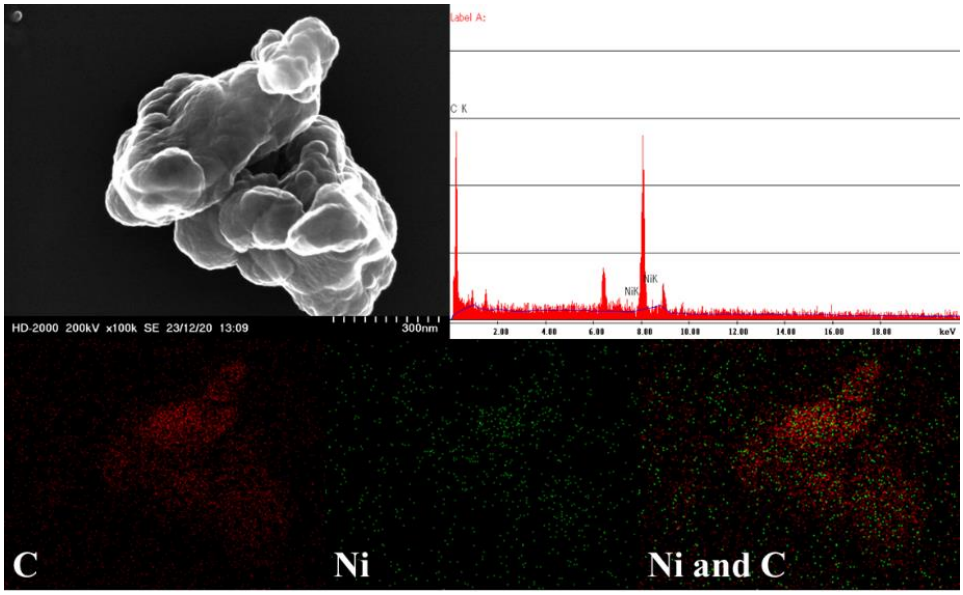

Figure S1. STEM image and EDS mapping of C and Ni for SiO_2-TiO_2@APTES-Ni(II)_10 mmol.

Substate scope for Kumada cross coupling reaction over SiO_2-TiO_2@APTES-Ni(II)_10 mmol

To investigate the scope of the reaction with SiO_2-TiO_2@APTES-Ni(II)_10 mmol, we performed the reactions using substrates with electron-donating and -withdrawing substituents at *meta* and *para* positions. As electron-donating and -withdrawing substituents, methyl and nitro groups were chosen, and the reactions were performed in the presence of SiO_2-TiO_2@APTES-Ni(II)_10 mmol under the optimal reaction conditions (50 °C and 6 h). As Table S1 demonstrates, the reactions gave the corresponding products in moderate to high yields.

Table S1. Substrate scope of Kumada cross coupling reaction catalysed by SiO_2-TiO_2@APTES-Ni(II)_10 mmol[a].

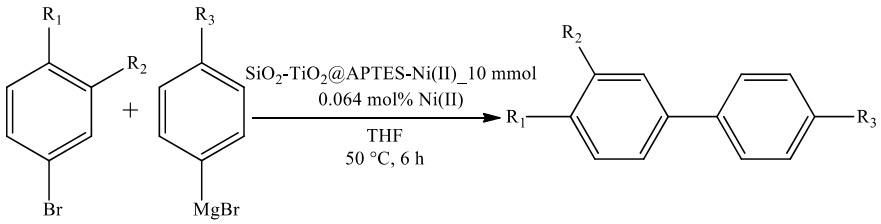

Entry	R_1	R_2	R_3	Product	Yield[b]
1	CH_3	H	H	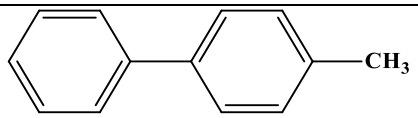	73
2	H	CH_3	H	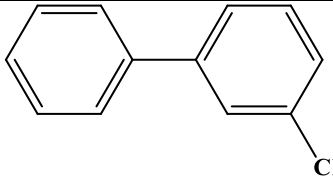	63

3	CH_3	H	CH_3	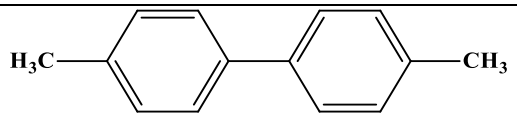	69
4	H	CH_3	CH_3	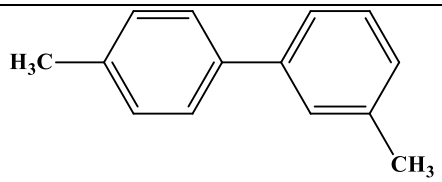	60
5	NO_2	H	H	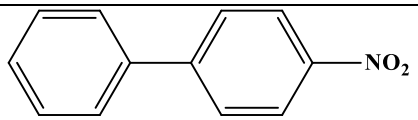	93
6	H	NO_2	H	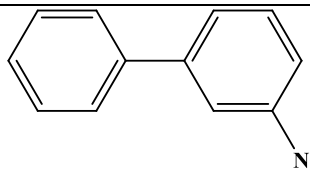	84
7	NO_2	H	CH_3	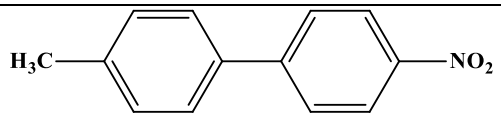	87
8	H	NO_2	CH_3	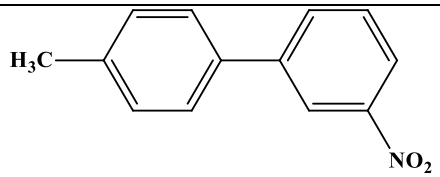	80

675 [a]Reaction conditions: catalyst, 0.1 g; reactants, arylmagnesium bromide and aryl bromide, 1

676 mmol each; solvent, deoxygenated THF, 2 mL; temperature, 50 °C; and time, 6 h.

677 [b]GC yield.

678

STEM-EDX mapping for the spent SiO_2-TiO_2@APTES-Ni(II)_10 mmol

Figure S2 shows STEM-EDX mapping of the spent catalyst, were compared with those of the fresh one in this figure. As the EDX mapping of the spent catalyst (Figure S2(e)), Ni species was slightly agglomerated after the repeated use. Therefore, it can be concluded that the agglomeration of Ni species as well as accumulation of the products on the catalyst caused the catalyst deactivation with repeated use.

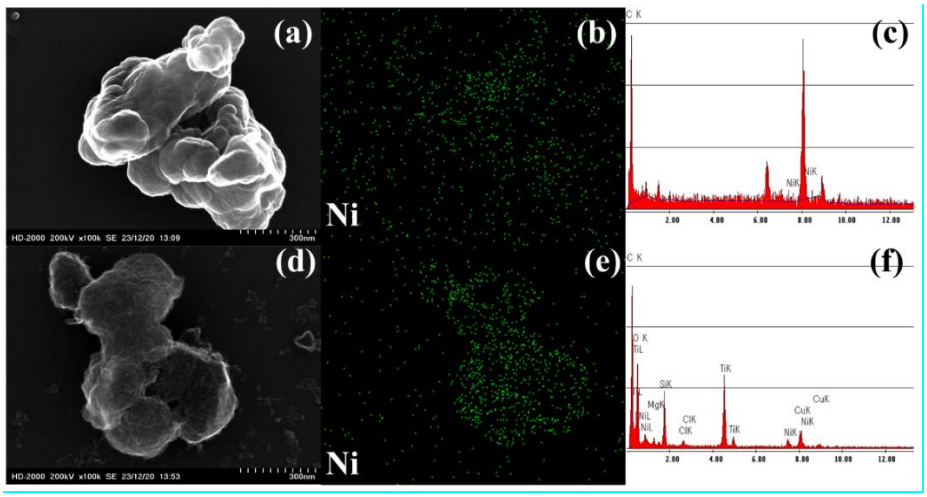

Figure S2. STEM images (a,d); EDX mappings (b,e); and EDS spectra (c,f).

(a, b, c) fresh SiO_2-TiO_2@APTES-Ni(II)_10 mmol and (d, e, f) the spent catalyst after the second reuse.